

{2-phases 2-reactions 1-catalyst} concept for the sustainable performance of coupled reactions

Philipp Schmid,¹ Gasper Jost,¹ Xaver Graß,¹ Didier Touraud,² Olivier Diat,³ Arno Pfitzner¹ and Pierre Bauduin^{3,*}

-
- 1 Institute of Inorganic chemistry, University of Regensburg, Universitätsstraße 31, 93053 Regensburg, Germany
2 Institute of Physical and Theoretical chemistry, University of Regensburg. Universitätsstraße 31, 93053 Regensburg, Germany
3 ICSM, CEA, CNRS, ENSCM, Univ Montpellier, 34199 Marcoule, France

Supporting Information

Table of Contents

1. Distribution of $PW_{12}O_{40}^{3-}$ depending on acidity/basicity and counter-cations	3
2. Benzylaldehyde synthesis	5
3. DR-13 degradation	7
4. Ag recovery	8
5. Ferrioxalate complexation reaction	14
6. Combined degradation of DR-13 and recovery of Ag	15
7. Experimental section	16
7.1 Chemicals	16
7.2 Sample preparation and extraction (distribution)/reaction processes	16
7.3 Quantitative analyses	17
7.4 1H -nuclear magnetic resonance (NMR).....	19
7.5 ^{31}P -nuclear magnetic resonance (NMR).....	19
7.6 UV/VIS measurements.....	19
7.7 Inductively coupled plasma-optical emission spectroscopy (ICP-OES)	19
7.8 X-ray powder diffraction (XRPD)	19
7.9 pH measurement	19
7.10 Scanning electron microscopy (SEM) – energy-dispersive X-ray (EDX) spectroscopy	20

7.11 Infrared (IR) spectroscopy	20
8. Bibliography.....	21

1. Distribution of $\text{PW}_{12}\text{O}_{40}^{3-}$ depending on acidity/basicity and counter-cations

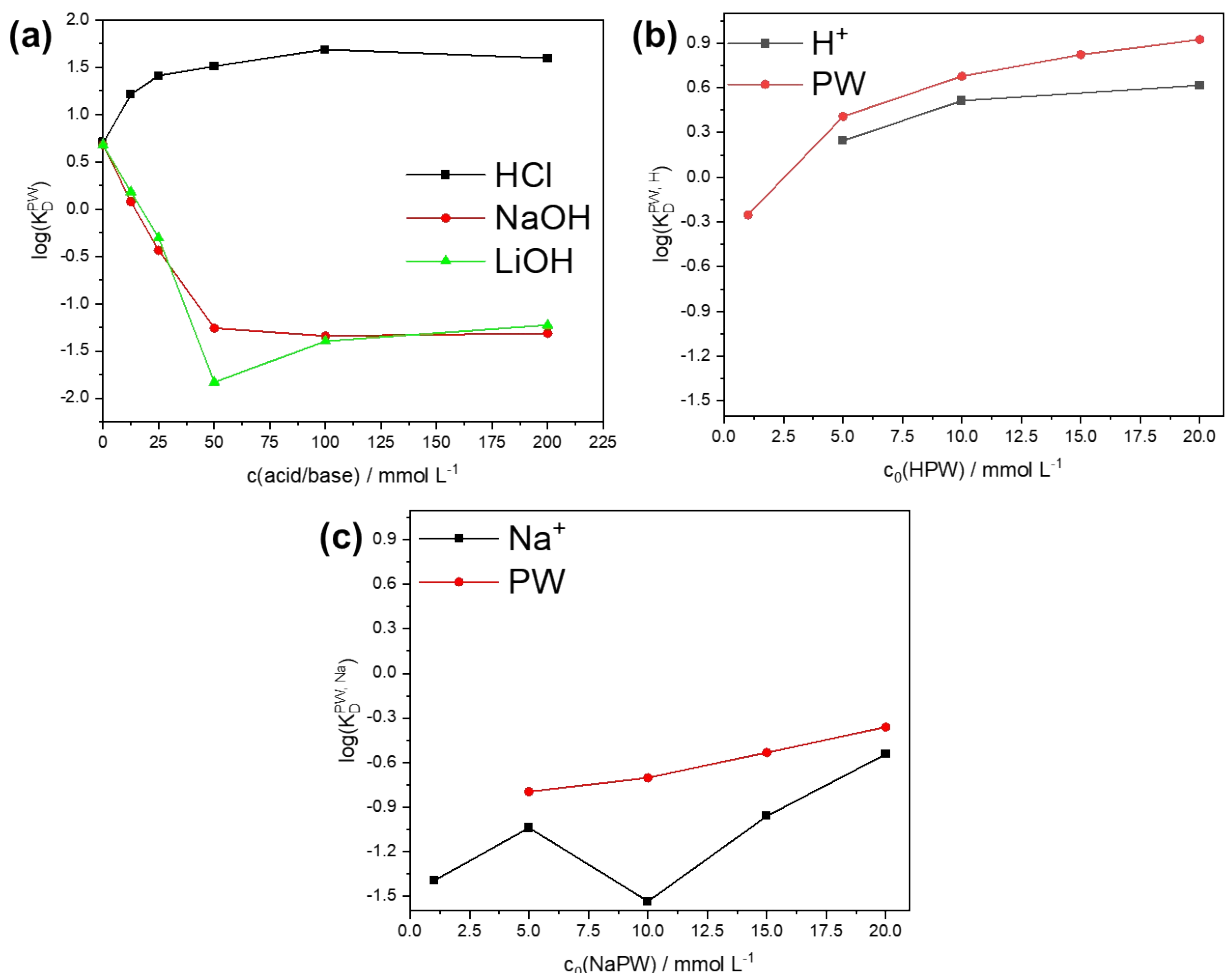


Figure S1. (a) shows the distribution of $c_0(\text{HPW}) = 10 \text{ mmol L}^{-1}$ to 1-OctOH as a function of acid (HCl) or base (NaOH, LiOH) concentration. Generally, the distribution coefficient increases with increasing acidity and decreases with increasing basicity. (b) and (c) show the distribution coefficient of PW, *cf.* Fig. 1 (manuscript) and of its counter-cation (b) H⁺ and (c) Na⁺. In case of HPW, both, the PW anion, and the H⁺ cation are extracted, whereas in case of NaPW, neither the PW anion, nor the Na⁺ cation is extracted to the organic phase in high yields.

Figure S1a shows the distribution coefficient of 10 mmol L^{-1} HPW from aqueous solution to the organic phase 1-OctOH as a function of acid or base concentration. Interestingly, the distribution coefficient increases from 0.67 to 1.6 upon the addition of 200 mmol L^{-1} HCl. In such high acidity media, it is known, that protons are in the close vicinity of the PW anion. It is likely, that H⁺ and PW form contact-ion pairs.¹⁻³ Therefore, species of the type $\text{H}_{3-x}\text{PW}_{12}\text{O}_{40}^{x-}$ ($x < 3$) are formed which provide a lower net charge than fully dissociated $\text{PW}_{12}\text{O}_{40}^{3-}$. Consequently, the POM appears less hydrophilic and more hydrophobic. This increased hydrophobicity is likely to lead to enhanced extraction to organic phases, such as 1-OctOH in our case.

The addition of 100 mmol L⁻¹ base, here LiOH/NaOH, leads to a strong decrease of the distribution coefficient (from 0.67 to approximately -1.25). As PW and other POMs are known as acid-catalysed condensation products, the speciation of them at different pH was intensively investigated.⁴⁻⁶ A general conclusion, that is drawn is that plenary PW₁₂O₄₀³⁻ is only stable at pH < 3. At higher pH, PW is known to degrade gradually to phosphate and tungstate (pH > 9) with several (lacunary) POM intermediates. As these degradation products are highly charged, they can be assumed as highly hydrophilic and therefore the distribution coefficient decreases to 0 %.

Figure S1b shows the distribution of HPW to 1-OctOH, *cf.* Fig. 1a (manuscript). Additionally, the distribution of H⁺ was investigated here. Interestingly, PW and H⁺ are distributed to a similar extent (around 0.6) in the organic phase. Hence, we prove here, the ion-pair formation of PW and H⁺. In case of the extraction of NaPW to 1-OctOH, we find only very low distributions (below -0.35) for both, the alkali metal cation and the POM anion, see Figure S1c. Summarized, we find the combination of H⁺ and PW₁₂O₄₀³⁻ the only cation-anion pair, that can be extracted from water to an organic alcohol phase. The extraction process requires (i) the low charge (density) of PW₁₂O₄₀³⁻, as well as (ii) high acidity in order to form POM-cation contact pairs.

2. Benzylaldehyde synthesis

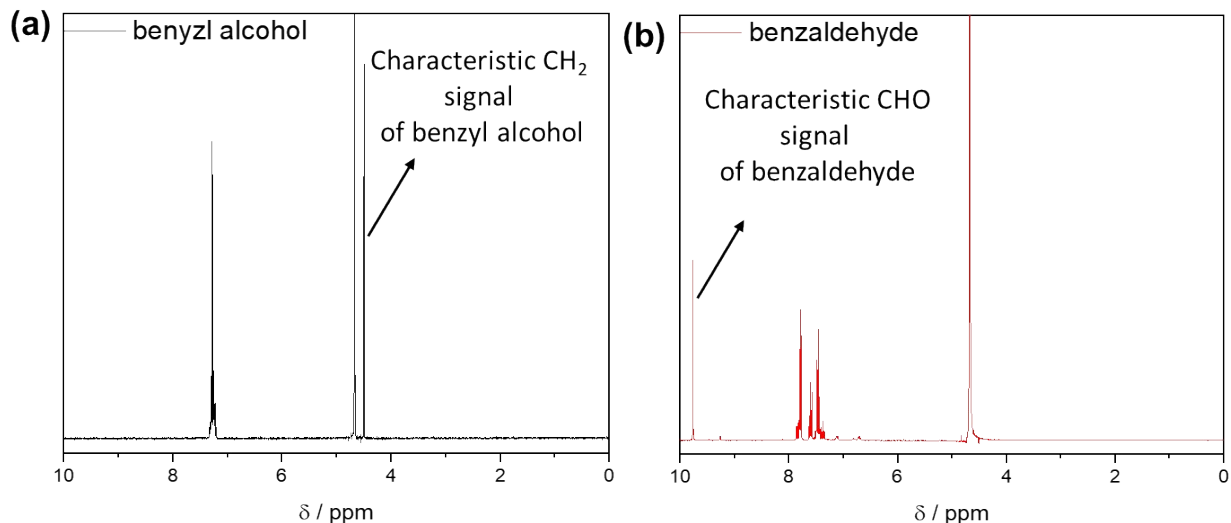


Figure S2. ¹H-NMR spectrum of (a) benzyl alcohol and (b) benzaldehyde in D₂O.

Figure S2a shows the ¹H-NMR spectrum of benzyl alcohol in D₂O (20 mmol L⁻¹). Benzyl alcohol produces a characteristic singlet at around 4.45 ppm stemming from the CH₂ moiety. The aromatic protons lead to a multiplet at 7.28 ppm. At 4.65 ppm the peak of D₂O arises. D₂O was chosen here as a solvent, to enhance the readability of the NMR spectra, as CDCl₃ (which was used in this study) produces a strong singlet in the region of the multiplet of aromatic protons.

Figure S2b shows the ¹H-NMR spectrum of benzaldehyde in D₂O (20 mmol L⁻¹). A characteristic singlet at around 9.78 ppm emerges due to the -CHO moiety in benzaldehyde. Different multiplets, due to e.g. ⁴J-coupling of the -CHO proton with aromatic protons, arise between 7.30 and 7.88 ppm. Again, the D₂O peak is located at 4.65 ppm.

In order to analyse the conversion of benzyl alcohol to benzaldehyde the ratio of singlet(9.78 ppm) : singlet(4.45 ppm) is investigated by integrating the reaction mixture spectra. This ratio is conclusive on the ratio benzaldehyde : benzyl alcohol in solution and therefore on the conversion of benzyl alcohol.

Table S1 summarizes the different integrals and the thereby calculated benzyl alcohol to benzaldehyde conversion.

Table S1. Integrals of the characteristic moieties in benzyl alcohol and benzaldehyde and the corresponding reaction equation.

time/h	Integral -CHO	Integral -CH ₂	Integral -CH ₂ normalized	conversion / %
0	0.00	1.00	0.50	0.00
5.5	0.25	9.15	4.58	5.57
14	0.79	12.53	6.26	12.68
23.5	0.76	7.38	3.69	20.62
48	1.10	7.50	3.75	29.47
72	1.88	10.62	5.31	35.32

3. DR-13 degradation

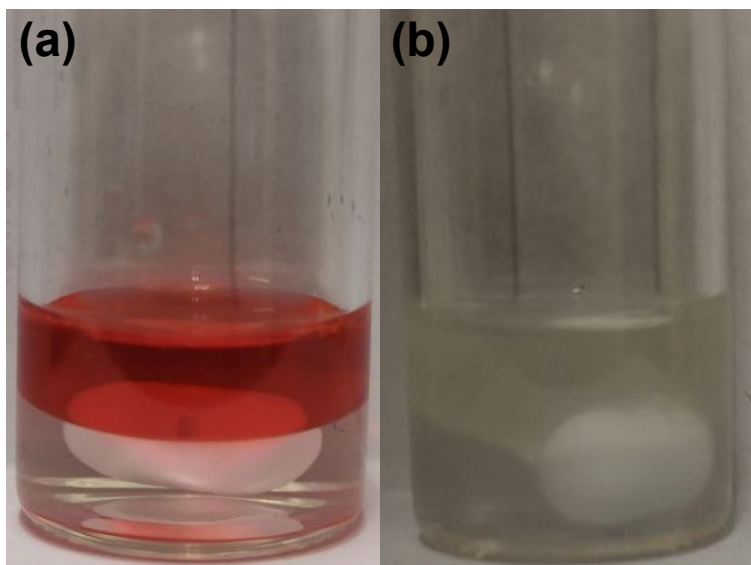


Figure S3. Images of the DR-13 degradation after (a) fresh preparation and (b) 12 h UV-light illumination. Whereas at initial conditions, the organic phase appears deeply red owing to the DR-13 dye and the aqueous phase is colorless, transparent, after the reaction the organic phase is less colored due to the degradation of DR-13.

Figure S3 provides images of the DR-13 degradation, where (a) shows the sample after fresh preparation and (b) shows the sample after 90 minutes UV illumination. The reactions conditions are recalled here: organic phase: 2-Me-2-HexOH, $c_{\text{org. phase}}(\text{DR-13}) = 1 \text{ mmol kg}^{-1}$, $c(\text{HPW}) = 10 \text{ mmol L}^{-1}$, UV light illumination: 365 nm, vigorous stirring. After fresh preparation (exclusively) the organic phase is deeply red coloured owing to the characteristic colour of DR-13. After 90 minutes reaction time, the organic phase appears (nearly) completely decoloured as DR-13 is successfully degraded.

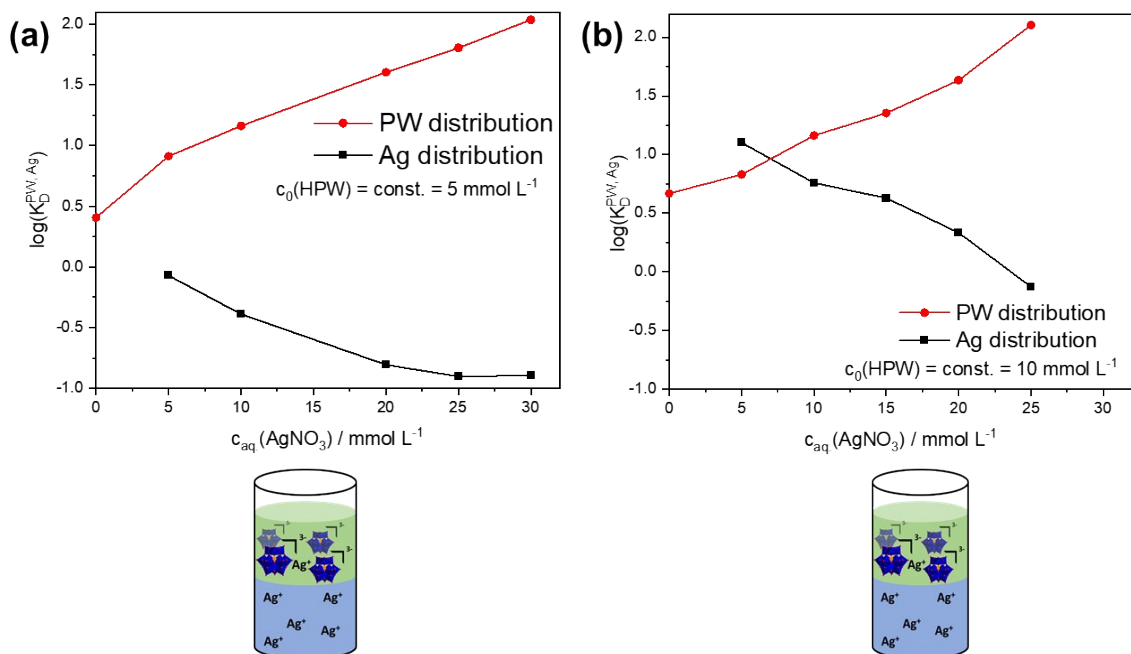


Figure S4. The extraction of AgNO₃ and (a) 5 mmol L⁻¹ and (b) 10 mmol L⁻¹ HPW in the biphasic system water:1-OctOH as a function of AgNO₃ concentration. At low AgNO₃ concentrations Ag⁺ is extracted to the organic phase together with the POM. At high AgNO₃ concentrations the PW anion is found mainly in the organic phase and Ag⁺ mainly in the aqueous phase.

4. Ag recovery

Figure S4 shows simultaneously the distribution of Ag⁺ (from AgNO₃) and PW (HPW) in the biphasic system water:1-OctOH. The c₀ concentration of HPW was constant at (a) 5 mmol L⁻¹ and (b) 10 mmol L⁻¹, respectively, whereas the concentration of AgNO₃ was varied. Interestingly, Ag⁺ is (partially) distributed in the organic phase at low AgNO₃ concentrations. For example, at 5 mmol L⁻¹ AgNO₃ the Ag⁺ distribution coefficients are -0.07 and 1.1 for (a) 5 mmol L⁻¹ and (b) 10 mmol L⁻¹ HPW, respectively. As Ag⁺ is a large cation (ionic radius 126 pm between the radii of Na⁺ (119 pm) and K⁺ (138 pm)⁸) it is likely that it may form a contact ion-pair with PW at low concentrations (according to Collins' concept⁹)¹⁰ that is extracted to the organic phase.

By increasing the AgNO₃ concentration the amount of distribution decreases. For example, at 25 mmol L⁻¹ AgNO₃ the distribution coefficients are -0.9 and -0.12 for (a) 5 mmol L⁻¹ and (b) 10 mmol L⁻¹ HPW, respectively. In order to guarantee, that PW is mainly distributed in the organic phase and Ag⁺ mainly in the aqueous phase (as demanded by the reaction setup) the concentrations for the model reaction in the manuscript have been determined as. c_{aq. phase} (AgNO₃) = 25 mmol L⁻¹ and added 5 mmol L⁻¹ HPW as catalyst.

Figure S5 shows images of the Ag recovery, with (a) after fresh preparation and (b) after 180 minutes UV-light illumination. The reactions conditions are recalled here: organic phase: 1-OctOH, $c_{\text{aq. phase}}(\text{AgNO}_3) = 25 \text{ mmol L}^{-1}$, $c(\text{HPW}) = 5 \text{ mmol L}^{-1}$, UV light illumination: 365 nm, vigorous stirring. After fresh preparation, two clear, transparent

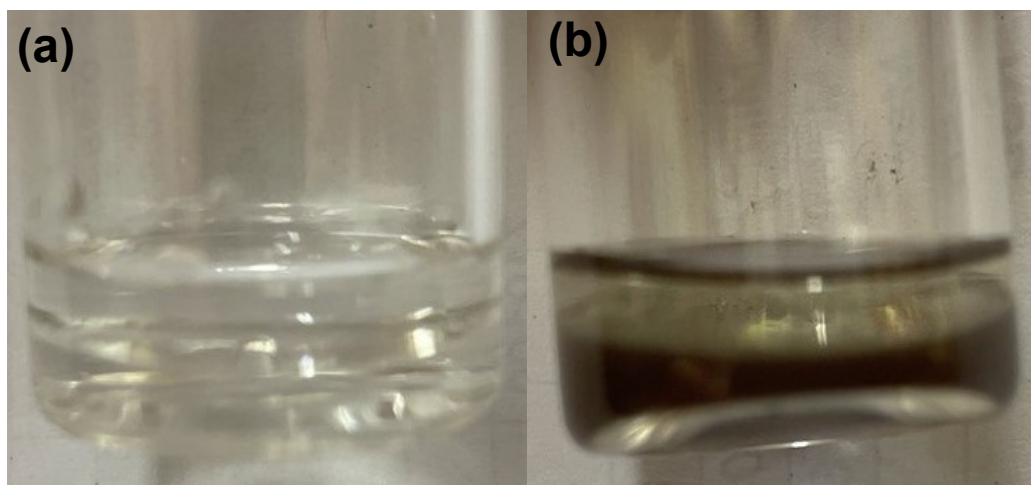


Figure S5. Images of the Ag recovery after (a) fresh preparation and (b) 180 minutes UV-light illumination. Whereas at initial conditions, two clear, transparent phases are observed, a silverish shade appears in the aqueous phase after the reaction. This shade arises from dispersed elemental silver.

phases are depicted. After 180 minutes UV-light illumination the bottom (aqueous) phase exhibits the characteristic silverish shade of dispersed elemental Ag.

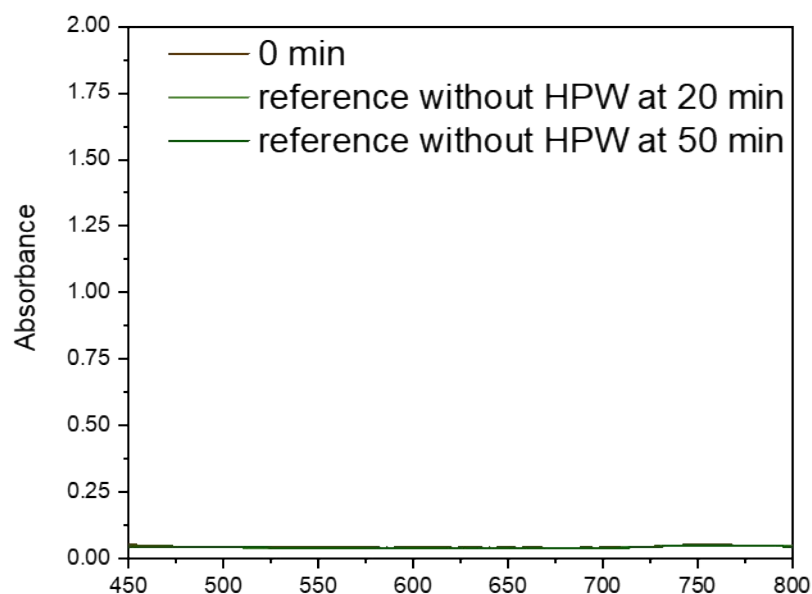


Figure S6. Reference UV/VIS spectra of the formation of Ag particles in the presented biphasic system (water:1-OctOH) in absence of the catalyst HPW. The absorbance/scattering is not increased in the observation window between 0 and 50 minutes of UV-illumination. The scale y-axis is set from 0 to 2 in order to have a good comparison to Fig. 4a in the manuscript.

A reasonable question to ask is on the nature of the produces silver as not only large, precipitate-like particles¹¹ can be formed by reduction of metal ions with photoreduced polyoxometalates, namely nano-particles. It was described and shown by diverse, that nano-particles of metals can be stabilized by POMs, that are adsorbed on the nano-particle surface.^{12,13} In 2002, it was the group of Papaconstantinou who published a landmark paper on the stabilization of metal (M) nano-particles (with M = Pd, Pt, Ag, Au).¹⁴ In their paper, the photoreduced form of Keggin-POMs is used to (i) reduce M⁺ species and (ii) to stabilized the synthesized M in nano-particles.

The formation of such POM stabilized nano-particles leads to several different “optical” features which distinguish the solution/dispersion from a dispersion of large, precipitate-like, particles:¹⁴

- (i) Due to the small size of the nano-particles, the solution/dispersion will appear yellow for Ag particles.
- (ii) The colloidal dispersion is stable for several months.
- (iii) The colloidal dispersion (Ag nano-particles) can be filtered in a 450 nm filter (PTFE) and no nano-particles, typically in the range of <100 nm, will be filtered.

In our case, the aqueous phase of the reaction mixture was strongly silverish, see Fig. S5, the product sedimented within only a tens of minutes to few hours and upon filtration with a 450 nm PTFE filter all product remained in the filter, while the filtrate was clear, transparent after filtration. This already indicates that no nano-particles, and instead large Ag particles, are formed.

In order to proof these observations, scanning electron microscopy (SEM) is performed on a representative sample of produced Ag, see Fig. S7 (a)-(d). All four SEM images (on different scales) do not show the presence of distinct, small nano-particles. Instead, intergrown particles of different sizes in the micrometer regime are observed. Such intergrown particles of ill-defined shape are striking for a rapid crystallization, which goes in line with the observation, that the product sediments quickly from solution.

In a next step, we probe the presence of HPW in the product sample. As a first

methodology, energy-dispersive X-ray (EDX) spectroscopy is performed. A typical EDX

spectrum of our product is shown in Fig. S7(e). Among the detection of C (carbon sample

carrier), O (pollution) and the product Ag, only a small signal appears for W and no signal

can be detected for P (central atom of the PW anion). The quantitative EDX analysis of

Ag, W and P is shown in Table S2 and reveals the composition 97 atom% Ag, 3 atom%

W and 0 atom% W. Note, that the absolute error may also decrease the amount of W to

2 atom%. Accordingly, the W/Ag ratio in our case is $W/Ag \approx 0.025$, while in other reports

the critical ratio to stabilize nano-particles with Keggin-POMs was reported to be between

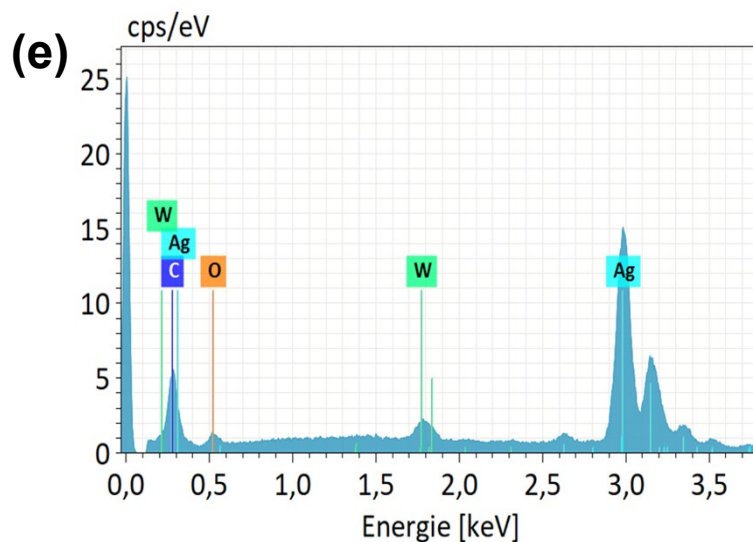
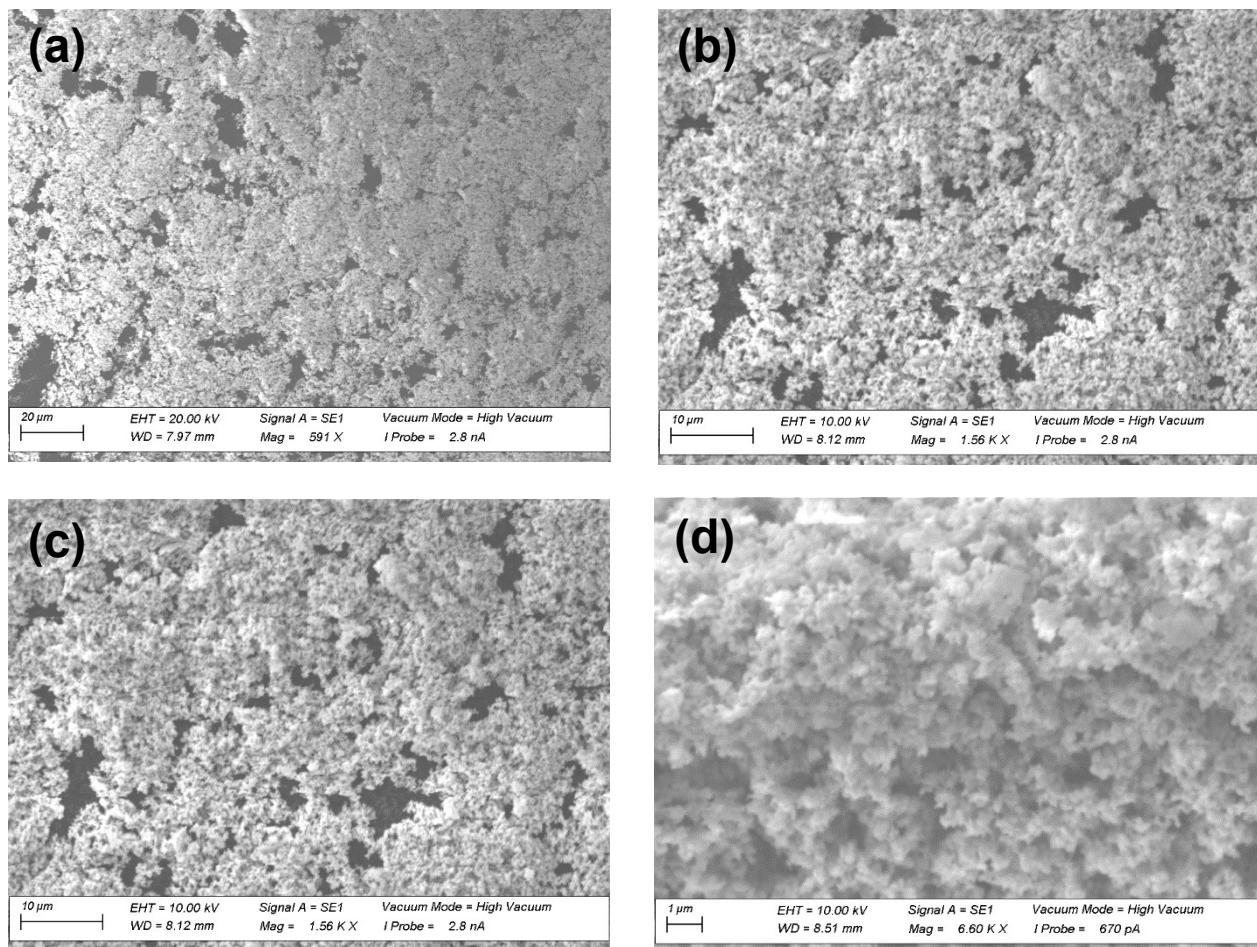


Figure S7. (a)-(d) Representative SEM images of the produced silver. (e) EDX measurement of the product indicating the presence of Ag (product), C (due to carbon sample holder matrix), O (different reasons: e.g. remaining water) and partially W(HPW).

0.12-0.18¹³ and even far above 1.¹² The here detected trace of W may be due to an

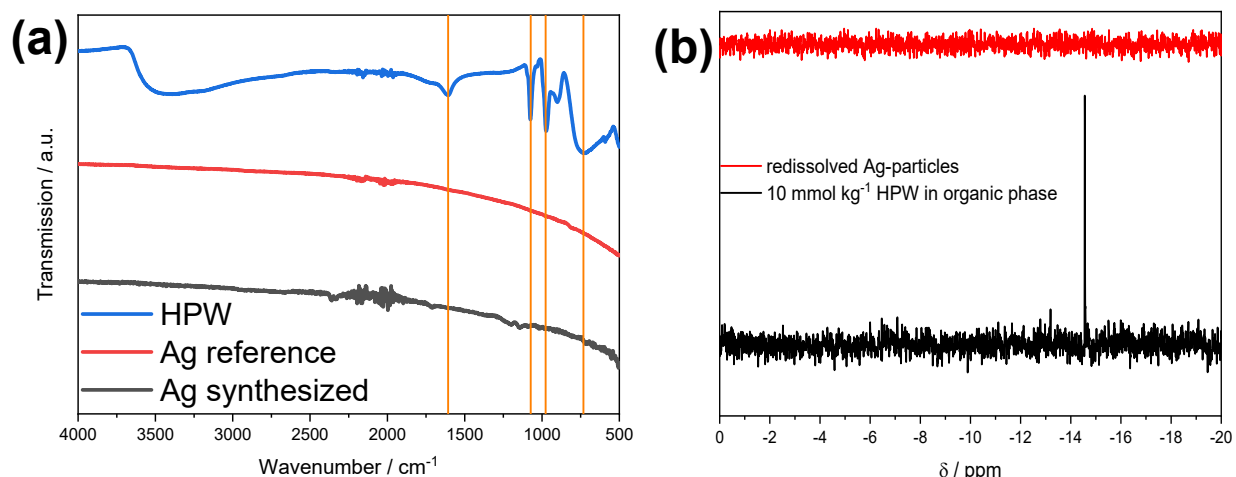


Figure S8. (a) IR spectra of the references HPW (blue) and Ag (red) and of our synthesized product (black). (b) ^{31}P -NMR spectra of a reference (black, 10 mmol kg^{-1} HPW in the organic phase) and of a sample of the redissolved product (red). Both methods indicate the absence of HPW.

incomplete washing procedure (3 times with deionized water) of the SEM/EDX sample.

Table S2. Evaluation of the EDX spectra showing that HPW is only available in traces in the product phase (Ag). This is further confirmed, as EDX measurements do not detect the signal of P (central atom of HPW).

Element	Element number	Netto counts	Atom / %	Absolute error / %
Ag	47	90955	97.40	8.75
W	74	5447	2.60	0.61
P	15	0	0.00	0.00

In order to further verify the absence of HPW in the Ag-product and therefore to exclude the formation of nano-particles, infrared (IR) spectroscopy is performed, see Fig. S8a. As references, spectra are recorded for HPW (blue) and a reference sample of Ag (red). The spectrum of our synthesized product corresponds perfectly to the spectrum of the Ag reference. If HPW would be present on the surface of nano-particles the signature of HPW would be recorded in the spectrum of our synthesized product (black).

As a last complementary technique, the presence of HPW on Ag-particles is checked by ^{31}P -NMR, see Fig. S8b. Therefore, a portion of the obtained product was redissolved in hot HNO_3 and a NMR-spectrum was recorded. While, a reference sample (black, 10 mmol kg^{-1} in the organic phase) produces a sharp singlet at around -14.6 ppm . This, or any other P-signals do not appear in the NMR-spectrum of the redissolved Ag, confirming the absence of HPW.

By combining, observations, SEM and three different spectroscopic techniques (EDX, IR, NMR), we conclude, that no HPW-stabilized Ag nano-particles are observed.

In his paper, Papaconstantinou gives the explanation, why here no nano-particles are observed. Nano-particles of M (with M = Pd, Pt, Ag, Au) can commonly be stabilized by the negative charge of POMs. The colloidal stability then can be described via the famous Derjaguin-Landau-Verwey-Overbeek (DLVO) theory.¹⁵ This theory, in its simplest consideration, comprises three different contributions, namely, the Born-repulsion, van-der-Waals attractions and Coulomb-repulsion. While the Born-repulsion and van-der-Waals attractions are more difficult to manipulate, the Coulomb repulsion is easy to control. Hence, it appears in all colloidal systems, that upon increasing the ionic strength, the Coulomb repulsion is decreased. This decrease in Coulomb repulsion leads to the irreversible coalescence, *i.e.* the thermodynamical instability of nano-particles. Therefore, Papaconstantinou finds the ionic strength in solution as the critical parameter, if nano-particles or large, precipitate-like, particles are observed.^{11,14} Only at very low ionic strength the Keggin-POM-stabilized nano-particle formation is possible. In our system: 5 mM HPW and 25 mM AgNO₃ an ionic strength, *I*, of $I \approx 0.1$ M is present. In comparison, Papaconstantinou reports on ionic strengths of $I \approx 0.01$ M to obtain nano-particles, *i.e.* a factor of one tenth, compared to our system.¹⁴ In conclusion, no POM-stabilized Ag nano-particles are here formed as a consequence of high ionic strength in solution.

5. Ferroin complexation reaction

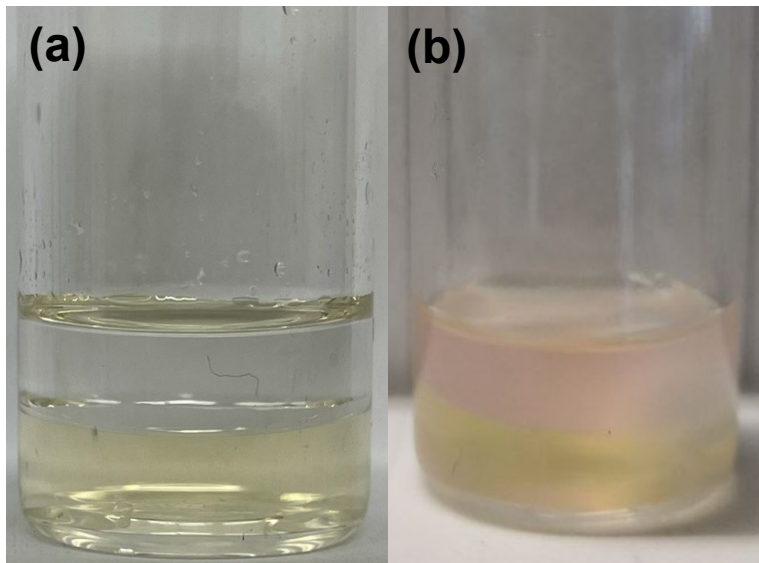


Figure S9. Images of the ferroin complexation after (a) fresh preparation and (b) 180 minutes UV-light illumination + 12 hours equilibration time. Whereas at initial conditions, the organic phase appears colorless, transparent the aqueous phase is light yellow (Fe^{3+} -ions in solution), after the reaction the organic phase is light red ($[\text{Fe}^{\text{II}}(\text{phen})_3]^{2+}$) and the aqueous phase remains light yellow (remaining Fe^{3+} -ions in solution).

Figure S9 shows images of the in-situ ferroin complexation, with (a) after fresh preparation and (b) after 90 minutes UV-light illumination + 12 hours equilibration time. The reactions conditions are recalled here: organic phase: 1-OctOH, $c_{\text{org. phase}}((1,10)\text{-phenanthroline}) = 0.5 \text{ mmol kg}^{-1}$, $c_{\text{aq. phase}}(\text{FeCl}_3) = 2 \text{ mmol L}^{-1}$, $c(\text{HPW}) = 10 \text{ mmol L}^{-1}$, UV light illumination: 365 nm, vigorous stirring. After fresh preparation the organic phase appears transparent, whereas the aqueous phase is light yellow coloured (Fe^{3+} -ions in solution). After 90 minutes UV-light illumination the bottom (aqueous) phase remains light yellow (excess Fe^{3+} -ions in solution) and the organic phase appears light red owing to the formation of $[\text{Fe}^{\text{II}}(\text{phen})_3]^{2+}$. After 12 h of equilibration time, the $[\text{Fe}^{\text{II}}(\text{phen})_3]^{2+}$ starts to precipitate leading to the turbidity obtained in Fig. S9

6. Combined degradation of DR-13 and recovery of Ag

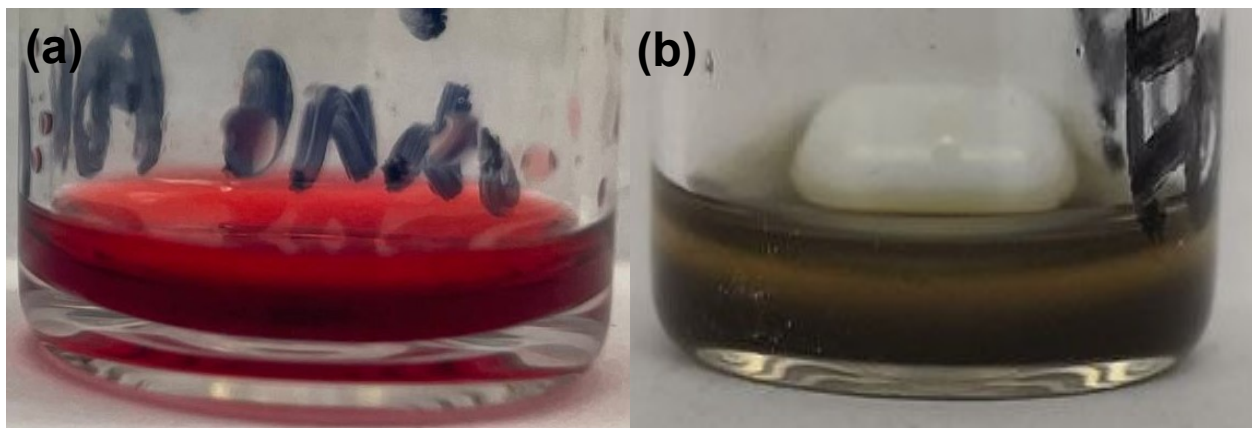


Figure S10. Images of the combined DR-13 degradation and Ag recovery after (a) fresh preparation and (b) 300 minutes UV-light illumination. Whereas at initial conditions, the organic phase appears deeply red owing to the DR-13 dye and the aqueous phase is colorless, transparent (solubilized AgNO_3), after the reaction the organic phase is less colored due to the degradation of DR-13 and the aqueous phase shows a silverish shade, indicating the formation of elemental Ag.

Figure S10 provides images of the simultaneous DR-13 degradation and Ag recovery, where (a) shows the sample after fresh preparation and (b) shows the sample after 300 minutes UV illumination. The reactions conditions are recalled here: organic phase: 2-Me-2-HexOH, $c_{\text{org. phase}}(\text{DR-13}) = 1 \text{ mmol kg}^{-1}$, $c_{\text{aq. phase}}(\text{AgNO}_3) = 25 \text{ mmol L}^{-1}$, $c(\text{HPW}) = 5 \text{ mmol L}^{-1}$, UV light illumination: 365 nm, vigorous stirring. After fresh preparation (exclusively) the organic phase is deeply red coloured owing to the characteristic colour of DR-13 and the aqueous phase appears colourless, transparent (solubilized AgNO_3). After 300 minutes reaction time, the organic phase appears (nearly) completely decoloured as DR-13 is successfully degraded and the aqueous phase provides the typical silverish shade owing to the formation of elemental silver.

7. Experimental section

7.1 Chemicals

Phosphotungstic acid hydrate ($\text{H}_3\text{PW}_{12}\text{O}_{40}$, MW = 2880 g/mol, 99.995% purity), silicotungstic acid hydrate ($\text{H}_4\text{SiW}_{12}\text{O}_{40}$, MW = 2878 g/mol) and sodium phosphotungstate ($\text{Na}_3\text{PW}_{12}\text{O}_{40}$, MW = 2946 g/mol) were purchased from Sigma Aldrich and used without further purification. Hydrochloric acid was purchased from Fischer Scientific. The hydrophobic alcohols 1-Hexanol, 1-Octanol and 2-Methyl-2-Hexanol were also purchased from Sigma Aldrich. The reaction chemicals benzyl alcohol, Disperse Red-13, AgNO_3 and FeSO_4 were obtained from Sigma Aldrich and used without further purification. FeCl_3 was purchased from Merck. (1,10)-phenanthroline was obtained from TCI Chemicals. ICP-OES standards were purchased from Bernd Kraft, Laborchemikalien. Milli-Q water was used with a conductivity lower than 10.5 $\mu\text{S}/\text{cm}$ and a total organic carbon content of 400 ppb.

7.2 Sample preparation and extraction (distribution)/reaction processes

The preparation of samples to determine the distribution coefficient followed a systematic procedure:

- 1) Aqueous stock solutions (concentration between 20 and 0 mmol L^{-1}) of POM (+additive) have been prepared. In order to precisely determine the POM concentration, a sample was taken, properly diluted and the concentration was analysed with ICP-OES.
- 2) 0.5 mL of the stock solutions were prepared into a 2 g reaction container (safe-lock Eppendorf cone)
- 3) 0.5 mL of an organic alcohol (1-Hexanol, 1-Octanol, 2-Methyl-2-Hexanol) were added to the reaction container
- 4) In order to increase the interface of the aqueous phase and the alcohol phase, the samples were shaken vigorously for three minutes
- 5) The samples were set on the table for five minutes to achieve phase separation
- 6) A sample of the aqueous phase was taken, properly diluted and the concentration was analysed with ICP-OES.

The preparation of all syntheses followed a systematic procedure:

- 1) Aqueous stock solutions (concentration: 10 or 5 mmol L^{-1}) of POM (+hydrophilic starting material for reaction) have been prepared
- 2) 0.5 mL of the stock solutions were prepared into a lockable 7 g reaction glass container

- 3) Stock solutions of an alcohol (+hydrophobic starting material for reaction) have been prepared
- 4) 0.5 mL of the organic alcohol stock solution were added to the reaction container
- 5) A magnetic stirring bar was set into the glass container and the glass container was put on a magnetic stirrer (~400 rpm)
- 6) A UV analysis lamp from Herolab GmbH, with a power of 6 W was used to initiate the different reactions. The excitation wavelength was in the near UV-region, *i.e.* with a monochromatic wavelength of 365 nm. Emission spectra of the lamp are available online on the webpage of the supplier Herolab (www.herolab.de/downloads/spezifikationen/Spektralkurven.pdf, 02.02.2022). The cylindrical lamp (length approximately 25 cm) was fixed in a special lamp holder. The lamp holder, including the lamp, were set close to the samples in a distance of approximately 2.5 cm. The length of 25 cm allows to perform multiple reactions (ca. 10) simultaneously in the used 7 g reaction glass container, guaranteeing the same flux of photons hitting a sample.
- 7) After fixed reaction times samples were taken and the reaction process was analysed via UV/VIS spectrometry (DR-13 recovery, Ag recovery, ferriin formation), ¹H-NMR (benzyl alcohol oxidation) or XRPD (dried Ag)

7.3 Quantitative analyses

Extraction process (Distribution coefficient determination)

The distribution coefficient $\log_{10}(K_D^X)$ of a compound X between an aqueous phase (aq.) and an organic phase (org.) can be described as

$$\log_{10}(K_D^X) = \log_{10}\left(\frac{c_{X, org.}}{c_{X, aq.}}\right) \quad (\text{S1})$$

As we only analysed the concentrations in the aqueous phase this term is extended to

$$\log_{10}(K_D^X) = \log_{10}\left(\frac{c_{0X} - c_{X, aq, after extraction.}}{c_{X, aq, after extraction.}}\right) \quad (\text{S2})$$

All extractions in the manuscript and the supporting information were calculated with Eq. S2.

Reaction analyses

All performed reactions were analysed (semi-)quantitatively. Here, we describe the analysing progress step by step.

1) Benzyl alcohol oxidation

In a first reaction we oxidized benzyl alcohol to benzaldehyde. Benzyl alcohol and benzaldehyde produce a characteristic multiplet (arising from the protons in the benzyl moiety) around 7.3 ppm in $^1\text{H-NMR}$. Moreover, benzyl alcohol gives a singlet (stemming from the CH_2 group around 4.6 ppm, whereas benzaldehyde produces a singlet (stemming from the H linked to the aldehyde functional group) around 10 ppm. $^1\text{H-NMR}$ allows to quantify the concentration of different H's by integrating NMR signals. Hence, samples were taken after certain reaction times, the characteristic peaks at 4.6 ppm (benzyl alcohol) and 10 ppm (benzaldehyde) were integrated and the quotient

$$\frac{c_{10 \text{ ppm}}}{c_{4.6 \text{ ppm}} + c_{10 \text{ ppm}}} = \frac{c_{\text{benzaldehyde}}}{c_{\text{benzyl alcohol, initial}}} \quad (\text{S3})$$

was calculated and informed quantitatively on the generation of benzaldehyde from benzyl alcohol.

2) DR-13 degradation

DR-13 produces a λ_{max} around 520 nm in UV/VIS spectroscopy. UV/VIS spectroscopy is known to follow Lambert-Beer's law and we can conclude on the DR-13 degradation by following the decreasing absorbance at λ_{max} with time. Consequently, we tracked the absorbance at 520 nm and calculated the degradation of DR-13.

3) Ag recovery

As proposed by Troupis *et al.* the recovery of Ag from Ag^+ leads to an increased solution turbidity, as Ag particles are formed.¹¹ Next to turbidimetry, UV/VIS spectrometry serves well to follow turbidity, as the basic absorbance level is elevated due to scattering and absorption. Absorbances were recalculated with dilution factors of the measured samples. Next to this semi-quantitative analysis XRPD was carried out on the dried Ag.

4) Ferroin complexation

Owing to its red colour (with Fe^{2+} as metal centre) ferroin produces a λ_{max} around 526 nm in UV/VIS spectroscopy. UV/VIS spectroscopy is known to follow Lambert-Beer's law and we can conclude on the ferroin formation by following the increasing absorbance at λ_{max} with time. Consequently, we tracked the absorbance at 526 nm and calculated the formation of ferroin. The total conversion (100 % formation) was established by using 0.5 mmol kg^{-1} (1,10)-phenanthroline in the organic phase (1-OctOH) and 2 mmol L^{-1} $\text{Fe}^{\text{II}}\text{SO}_4$.

7.4 ¹H-nuclear magnetic resonance (NMR)

Solution ¹H-NMR spectra were recorded (at room temperature) with an Avance300 (Bruker) spectrometer using tetramethyl silane as an internal standard. Chemical shifts (δ) are provided in parts per million (ppm) and coupling constants (J) are reported in Hertz (Hz). CDCl₃ was used as solvent.

7.5 ³¹P-nuclear magnetic resonance (NMR)

Solution ³¹P-NMR spectra were recorded (at room temperature) with an Avance400 (Bruker) spectrometer using 85 % phosphoric acid as an internal standard. Chemical shifts (δ) are provided in parts per million (ppm) and coupling constants (J) are reported in Hertz (Hz). D₂O was used as solvent.

7.6 UV/VIS measurements

UV/VIS measurements were carried out (at room temperature) on a Infinite M Nano+ from Tecan Trading AG. The measurements were executed in 1 cm quartz glass cuvettes and the samples were appropriately diluted with acetone (organic phase analysis) and water (aqueous phase analysis) and the absorption was therefore recalculated.

7.7 Inductively coupled plasma-optical emission spectroscopy (ICP-OES)

An ICP spectrometer, Ametek, Spectro, Spectroblue was used to determine metal concentrations in aqueous solution. Therefore, calibration curves were established using ICP-OES standards from Bernd Kraft, Laborchemikalien. The samples were appropriately diluted with milli-Q water and measured.

7.8 X-ray powder diffraction (XRPD)

XRPD measurements were carried out with a STOE Stadi P diffractometer with monochromatic Cu-K _{α 1} radiation ($\lambda = 0.1540598$ nm, Ge monochromator, Mythen 1K detector). The Ag-sample was measured at room temperature in a sealed glass capillary (1 mm) in a 2 θ range from 10 to 80 °. The WinXPow software was used to process the data.¹⁶

7.9 pH measurement

pH measurements were performed with a conventionally calibrated pH meter from Schott Instruments Analytics (ProLab 2000). Recalculation of c(H⁺) allowed to investigate the distribution of H⁺ in a biphasic system.

7.10 Scanning electron microscopy (SEM) – energy-dispersive X-ray (EDX) spectroscopy

Scanning electron microscopy-energy-dispersive X-ray (SEM-EDX) (Zeiss EVO MA 15 with Bruker XFlash Detector 630M) at 20 and 10 kV was applied to image Ag samples on a microscopic range and demonstrate the elemental composition and distribution along samples.

7.11 Infrared (IR) spectroscopy

Fouriertransform-Infrared (FT-IR) spectra were recorded in the range of 4000 – 500 cm^{-1} using a Varian 670 FT-IR spectrometer with a PIKE GladiATR extension.

8. Bibliography

- (1) Chaumont, A.; Wipff, G. Ion Aggregation in Concentrated Aqueous and Methanol Solutions of Polyoxometallates Keggin Anions: The Effect of Counterions Investigated by Molecular Dynamics Simulations. *Phys. Chem. Chem. Phys.* **2008**, *10* (46), 6940–6953. <https://doi.org/10.1039/b810440a>.
- (2) Bera, M. K.; Qiao, B.; Seifert, S.; Burton-Pye, B. P.; Olvera De La Cruz, M.; Antonio, M. R. Aggregation of Heteropolyanions in Aqueous Solutions Exhibiting Short-Range Attractions and Long-Range Repulsions. *J. Phys. Chem. C* **2016**, *120* (2), 1317–1327. <https://doi.org/10.1021/acs.jpcc.5b10609>.
- (3) Antonio, M. R.; Bera, M. K. PH-Dependent Interactions between Keggin Heteropolyanions in Dilute Solutions. *Eur. J. Inorg. Chem.* **2019**, *2019* (3), 367–373. <https://doi.org/10.1002/ejic.201801165>.
- (4) Rompel, A.; Gumerova, N. I. Polyoxometalates in Solution: Speciation under Spotlight. *Chem. Soc. Rev.* **2020**, *49*, 7568–7601. <https://doi.org/10.1039/d0cs00392a>.
- (5) Zhu, Z.; Tain, R.; Rhodes, C. A Study of the Decomposition Behaviour of 12-Tungstophosphate Heteropolyacid in Solution. *Can. J. Chem.* **2003**, *81* (10), 1044–1050. <https://doi.org/10.1139/v03-129>.
- (6) Maksimovskaya, R. I.; Maksimov, G. M. ³¹P NMR Studies of Hydrolytic Conversions of 12-Tungstophosphoric Heteropolyacid. *Coord. Chem. Rev.* **2019**, *385*, 81–99. <https://doi.org/10.1016/j.ccr.2019.01.014>.
- (7) Kozik, M.; Hammer, C. F.; Baker, L. C. W. NMR of ³¹P Heteroatoms in Paramagnetic One-Electron Heteropoly Blues. Rates of Intra- and Intercomplex Electron Transfers. Factors Affecting Line Widths. *J. Am. Chem. Soc.* **1986**, *108* (24), 7627–7630. <https://doi.org/10.1021/ja00284a028>.
- (8) Shannon, R. D. Revised Effective Ionic Radii in Halides and Chalcogenides. *Acta Crystallogr.* **1976**, *A32* (A32), 751. <https://doi.org/10.1107/S0567739476001551>.
- (9) Collins, K. D.; Neilson, G. W.; Enderby, J. E. Ions in Water: Characterizing the Forces That Control Chemical Processes and Biological Structure. *Biophys. Chem.* **2007**, *128* (2–3), 95–104. <https://doi.org/10.1016/j.bpc.2007.03.009>.
- (10) Misra, A.; Kozma, K.; Streb, C.; Nyman, M. Beyond Charge Balance: Counter-Cations in Polyoxometalate Chemistry. *Angew. Chemie - Int. Ed.* **2019**, *59* (2), 596–612. <https://doi.org/10.1002/anie.201905600>.
- (11) Troupis, A.; Hiskia, A.; Papaconstantinou, E. Photocatalytic Reduction — Recovery of Silver Using Polyoxometalates. *Appl. Catal. B Environ.* **2003**, *42*, 305–315. [https://doi.org/10.1016/S0926-3373\(02\)00264-3](https://doi.org/10.1016/S0926-3373(02)00264-3).
- (12) Wang, Y.; Weinstock, I. Polyoxometalate-Protected Metal Nanoparticles: Synthesis, Structure and Catalysis. In *Polyoxometalate Chemistry*; 2013; pp 1–47. https://doi.org/10.1142/9789814458986_0001.
- (13) Suo, L.; Gao, W.; Du, Y.; Wang, R.; Wu, L.; Bi, L. Preparation of Polyoxometalate Stabilized Gold Nanoparticles and Composite Assembly with Graphene Oxide: Enhanced Electrocatalytic Performance. *New J. Chem.* **2015**, *40* (2), 985–993. <https://doi.org/10.1039/C5NJ01983D>.
- (14) Troupis, A.; Hiskia, A.; Papaconstantinou, E. Synthesis of Metal Nanoparticles by Using Polyoxometalates as Photocatalysts and Stabilizers. *Angew. Chemie - Int.*

Ed. **2002**, *41* (11), 1911–1914. [https://doi.org/https://doi.org/10.1002/1521-3773\(20020603\)41:11<1911::AID-ANIE1911>3.0.CO;2-0](https://doi.org/https://doi.org/10.1002/1521-3773(20020603)41:11<1911::AID-ANIE1911>3.0.CO;2-0).

- (15) Isrealachvili, J. *Intermolecular and Surface Forces*, 3rd ed.; Elsevier, Ed.; Academic Press: London, 2011.
- (16) Stoe & Cie GmbH, D. WinXPOW Version 3. 2014.